ACS APPLIED MATERIALS & INTERFACES

Research Article

www.acsami.org

Polyvinyl Alcohol-Cellulose Nanofibrils-Graphene Oxide Hybrid Organic Aerogels

Alireza Javadi,[†,‡] Qifeng Zheng,[‡,§] Francois Payen,[‡,§] Abdolreza Javadi,[§] Yasin Altin,[‡,§] Zhiyong Cai,[⊥] Ronald Sabo,[⊥] and Shaoqin Gong*[,†,‡,§]

[†]Department of Biomedical Engineering, [‡]Wisconsin Institute for Discovery, and [§]Material Science Program, University of Wisconsin, Madison, Wisconsin, United States

[⊥]Forest Products Laboratories, U.S. Department of Agriculture, Madison, Wisconsin, United States

Supporting Information

ABSTRACT: Hybrid organic aerogels consisting of polyvinyl alcohol (PVA), cellulose nanofibrils (CNFs), and graphene oxide nanosheets (GONSs) were prepared using an environmentally friendly freeze-drying process. The material properties of these fabricated aerogels were measured and analyzed using various characterization techniques including compression testing, scanning electron microscopy, thermogravimetric (TGA) analysis, Brunauer–Emmet–Teller (BET) surface area analysis, and contact angle measurements. These environmentally friendly, biobased hybrid organic aerogels exhibited a series of desirable properties including a high specific compressive strength and compressive failure strain, ultralow density and thermal conductivity, good thermal stability, and moisture resistance, making them potentially useful for a broad range of applications including thermal insulation.

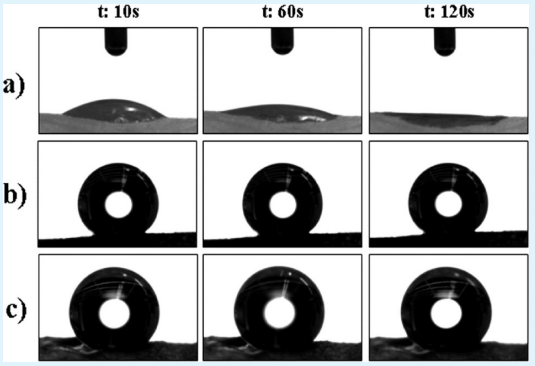

KEYWORDS: *organic aerogels, cellulose nanofibrils, graphene oxide, nanocomposites, thermal conductivity, hydrophobicity*

INTRODUCTION

Aerogels are lightweight materials that have drawn significant attention because of their combination of unique properties including a high porosity (typically 95%–99%), low density (typically less than 400 kg/m^3), high specific surface area, excellent thermal, acoustic, and electrical conductivities, and low dielectric constant.[1] Over the past 70 years, researchers have mostly focused on developing inorganic aerogels such as silica, clay, and metal oxide aerogels.[2−4] For instance, NASA has developed a series of silica-based inorganic aerogels for various space applications such as launch vehicles, space shuttle upgrades, interplanetary propulsion, space suits, and life support equipment.[5−11] Various types of inorganic-based aerogels have also been developed and commercialized for applications in the structural insulation, clothing, aviation, automotive, and aerospace industries. However, inorganic (mainly silica) aerogels often suffer from intrinsic brittleness, which consequently limits their use in applications where both high toughness and strength are required. As such, there is an increasing interest in developing unique organic aerogels with superior properties.[12−15]

Recently, nanocellulose-based aerogels have been actively studied.[16−22] Cellulose nanofibrils (CNF)-based aerogels have demonstrated high surface areas and excellent flexibility and deformability due to the entanglement of high-aspect-ratio CNFs and the presence of strong hydrogen bonds.[21] CNFs are derived from cellulose, which is an abundant biomass. Cellulose is one of three predominant components in lignocellulosic biomass; hemicelluloses and lignin are the other two. Unlike petroleum-based resources, lignocellulosic biomass is renewable and sustainable. Furthermore, its three components can be readily separated using mature technologies.[23,24] CNFs can be prepared from cellulose via various techniques,[25−29] including (1) processing of macroscopic fibers under high shear mechanical stress;[25,26] (2) 2,2,6,6,-tetramethylpiperidine-1-oxyl (TEMPO)-mediated oxidation;[29] or (3) enzymatic hydrolysis of macroscopic fibers followed by homogenization under high shear mechanical stress.[27,28] CNFs produced from the aforementioned methods form hydrogels in water, even at very low concentrations (<0.5 wt %).[27−29] CNF aerogels are fabricated by removing the interstitial liquid and replacing it with dry air. Special drying methods, such as supercritical drying or freeze-drying, are needed to avoid destroying the integrity of the network structure due to the high surface tension or capillary pressure between the water and the hydrogel network. Freeze-drying is an inexpensive, easy, and environmentally friendly method that can be used in the mass production of aerogels. Unlike the supercritical drying method, freeze-drying does not require multistep and time-consuming solvent exchange procedures and delicate handling of the gels.[30]

Received: January 25, 2013
Accepted: May 28, 2013
Published: June 24, 2013

Despite their remarkable characteristics, such as their extremely low density (5−20 kg/m^3) and deformability, CNF aerogels suffer from inferior strength and modulus as compared to their inorganic counterparts. Herein, we report a new type of CNF-based hybrid organic aerogel comprised of a CNF skeleton in combination with a water-soluble thermoplastic polymer (i.e., polyvinyl alcohol (PVA)) and graphene oxide nanosheets (GONSs) (abbreviated as PVA/CNF/GONS), which could overcome these deficits. In addition, the effects of silanization on the surface properties of the CNF-based aerogels were extensively studied. PVA is an inexpensive polymer that possesses desirable properties such as water solubility, biocompatibility, and biodegradability.[31] GONSs were chosen as the second nanofiller in this hybrid organic aerogel system because they are water-soluble and have excellent mechanical properties, large surface-to-volume ratios, and a large amount of oxygen atoms on their surface, thus enabling the formation of strong hydrogen bonds among the three components—i.e., PVA, CNF, and GONS. Freeze-drying was employed to fabricate these novel organic aerogels as it is inexpensive, easy, scalable, and capable of producing high-quality components in any desired geometry. These hybrid organic aerogels demonstrated excellent mechanical, thermal, and surface properties, hence making them potentially useful for a wide range of applications including flexible thermal insulations in both residential and commercial construction, aerospace, and commercial aircrafts.

EXPERIMENTAL SECTION

Preparation of Cellulose Nanofibrils (CNFs). TEMPO-oxidized CNFs used in this study were prepared according to the work reported by Saito et al.[29] Bleached eucalyptus pulp fibers were carboxylated using 2,2,6,6-tetramethylpiperidine-1-oxyl (TEMPO) (>96%, Sigma Aldrich), sodium chlorite (Sigma Aldrich), and sodium hypochlorite (Sigma Aldrich) as the reactants at 60 °C for 48 h. TEMPO oxidized pulp fibers were then washed thoroughly using distilled water and homogenized in a disk refiner to break apart fibril bundles. The fiber slurry was diluted to facilitate separation of coarse and fine fractions by centrifugation at 12000G, and the coarse fraction was rejected. The nanofiber suspension was concentrated to a solid content of approximately 0.4% using ultrafiltration. A final refining step was performed, in which the nanofiber suspension was passed once through an M-110EH-30 Microfluidizer (Microfluidics, Newton, MA) with 200- and 87 μm chambers in series. Further characterization of the CNFs is described in the Supporting Information.

Preparation of Graphene Oxide Nanosheets (GONSs). GONSs were prepared from purified natural graphite powder using an improved Hummer's method reported by Marcano et al.[32] Briefly, 1 g of graphite flakes (Sigma Aldrich) and 6 g of $KMnO_4$ (Sigma Aldrich) were added into a H_2SO_4/H_3PO_4 (Sigma Aldrich) mixture (135 mL:15 mL). The resulting mixture was stirred at 50 °C for 12 h. Afterward, the mixture was cooled to room temperature and then poured onto a mixture of 200 mL of ice and 1 mL of 30% H_2O_2 (Sigma Aldrich). The graphite oxide was washed and centrifuged with ethanol, HCl, and water sequentially until the pH level was 7. Thereafter, the supernatant was decanted away. The remaining solid was filtered over a PTFE membrane (0.45 μm pore size) and vacuum-dried overnight at room temperature.

Preparation of Cross-Linked PVA/CNF/GONS Aerogels. PVA solution (2.0 mL, 10%) (Sigma Aldrich), CNF solution (4.0 mL, 0.50%), 20 mg of GONSs, and desired amounts of water were mixed and vigorously stirred in a flask for 1 h. Then, glutaraldehyde solution (80 μL, 25% in H2O) (Grade II, Sigma Aldrich) and sulfuric acid (8 μL, 5.0−10.0%) (Sigma Aldrich) were added to the above solution, and were stirred for 1 h. At the final stage, the mixture was sonicated in an ultrasonic bath for 10 min. The resulting aqueous gels were transferred into aluminum pans and cross-linked in a vacuum oven at 75 °C for 3 h. The cross-linked gels were precooled to 4 °C in the fridge overnight and then quenched at −78 °C in dry ice−acetone solution. The frozen samples were freeze-dried in a lyophilizer at −87.0 °C and 0.0014 mBar vacuum for three days. The resulting aerogels were then stored in a desiccator for further characterization. A detailed description of the preparation methods for various formulations is provided in the Supporting Information section.

Surface Modification of Cross-Linked PVA/CNF/GONS Aerogels. The surface modification of the PVA/CNF/GONS aerogels was carried out by chemical vapor deposition using two different silane compounds (silane 1, (tridecafluoro-1,1,2,2-tetrahydrooctyl trichlorosilane) (Gelest Inc.); and silane 2, (4-(trifluoromethyl-tetrafluorophenyl) triethoxysilane) (Gelest Inc.). The chemical structures of the silane compounds are schematically shown in Figure 1. A small glass vial containing one of the selected silane

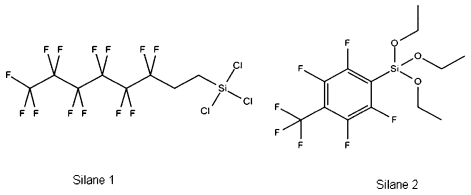

Figure 1. Schematic representation of the silane compounds used for the surface treatment of the PVA/CNF/GONS aerogels. Silane 1, tridecafluoro-1,2,2-tetrahydrooctyl trichlorosilane; and silane 2, 4-trifluoromethyl-tetrafluorophenyl triethoxysilane.

compounds together with the aerogel samples were placed in a large glass jar, which was heated in vacuum oven at 100 °C for 3 days. To remove the excess unreacted silane, the surface-treated aerogels were kept in a vacuum oven at room temperature until the vacuum level reached 3×10^{-2} mbar or less.

Characterization Methods. For each type of characterization described below, at least three specimens were measured for each sample and the average results were reported. The densities of the aerogels were calculated based on the measurements of their masses and dimensions. Compression testing was carried out by a dynamic mechanical analyzer (DMA Q800, TA Instruments, USA) at room temperature. The microstructures of the aerogels were investigated via a scanning electron microscope (SEM, LEO GEMINI 1530) with a field emission electron gun. The specific surface areas were determined by a Gemini (Micromeritics, USA) surface area analyzer at −196 °C using the Brunauer−Emmet−Teller (BET) method. Thermal stability measurements were carried out using a thermogravimetric analyzer (TGA, Q 50 TA Instruments, USA). The bulk thermal conductivity was measured using a thermal constants analyzer (ThermTest TPS 2500 S) following an ISO standard (ISO/DIS 22007−2.2). A contact angle goniometer (OCA 15/20, Future Digital Scientific Corp., USA) was used for the contact angle measurements that were carried out at room temperature with water. The contact angles were measured at three different positions on each sample. The values reported were measured at 10, 60, and 120 s after deposition of the droplets. The densities of the aerogels were determined by measuring their weight and volume without deforming the soft specimens. The X-ray diffraction (XRD) patterns for different CNFs were measured with a Bruker/Siemens Hi-Star 2d Diffractometer (Bruker AXS, Madison, WI, USA) using CuKa radiation generated at 40 kV and 30 mA. The X-ray scattering was detected with 2θ ranging from 2 to 40° at a scanning rate of 4°/min. The Raman measurements were performed at room temperature using a Thermo Scientific DXR Raman Microscope at a 532 nm laser excitation level.

RESULTS AND DISCUSSION

Compression Testing of Aerogels. Figure 2 shows the densities of the various aerogel samples made from CNFs, GONSs, and PVA. The densities of various aerogels ranged

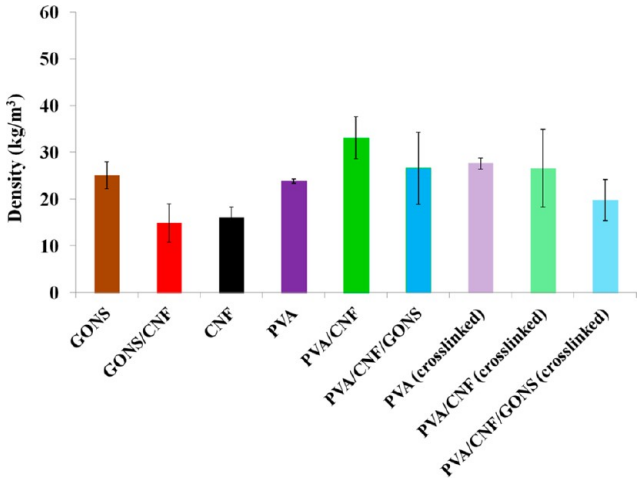

Figure 2. Densities of the aerogels made of various formulations consisting of CNFs, GONSs, and PVA that are either cross-linked or non-cross-linked.

from 15 to 35 kg/m^3. The specific compressive strength of the aerogels was calculated by dividing its ultimate compressive stress at 80% strain by its density.

The compressive behaviors of a series of aerogels made of CNFs, GONSs, and PVA that were either cross-linked or non-cross-linked are shown in Figure 3. The mechanical properties

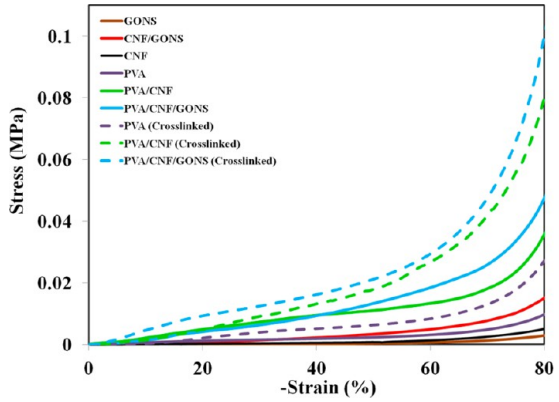

Figure 3. Compressive behaviors of aerogels made of various formulations consisting of CNFs, GONSs, and PVA that were either cross-linked or non-cross-linked.

of aerogels can be influenced by many factors including composition/formulation, microstructure, and relative densities. The material properties of the various components forming the aerogels including CNFs, GONSs and PVA in this case can also affect the mechanical properties of the aerogels. As discussed earlier, CNFs can be prepared via different methods leading to CNFs with different morphology, structure, and hence material properties.[25−29] For instance, it was reported that CNFs prepared via enzymatic hydrolysis could form very strong aerogels due to the strong entanglement between these long and flexible CNFs.[21,27] A number of studies also demonstrated that the mechanical properties of the aerogels (e.g., compressive strength and elastic modulus) and their relative densities exhibited a power-law relationship with the exponent typically ranging from 2 to 4, depending on the specific microstructure of the aerogel network.[33−35]

The ultimate compressive stress of the aerogel (0.014 MPa) comprised of both GONSs and CNFs at 80% strain was more than three times higher than that of the CNF aerogel (0.004 MPa). This dramatic increase may be attributed to the strong interactions between the GONSs and CNFs via hydrogen bonding. Moreover, the addition of PVA further increased the ultimate compressive stress at 80% strain of the aerogel from 0.014 to 0.1 MPa. This drastic improvement (more than 800%) can be attributed to PVA's long polymeric chains resulting in high density hydrogen bonding to CNFs and GONSs.[36−39]

Reinforcing structurally weak aerogels using polymers and/or other type of nanoparticles has been reported previously in a number of studies. For instance, silica-based aerogels have been reinforced by various types of polymers including isocyanates,[6,7] acrylates,[40] and epoxy[10] to improve their mechanical properties and load bearing capabilities. In addition, Schiraldi et al. reported a number of techniques including in situ polymerization of N-isopropylacrylamide,[41] addition of cellulose nanowhiskers[42] or short-cut natural fiber,[36] and incorporation of PVA[43,44] to reinforce clay-based aerogels. Bandi et al. investigated the effects of adding PVA on the glass transition temperature and crystallinity of the resulting clay-based aerogels.[43] Hostler et al. reported that incoporation of PVA enhanced the mechanical strength of the clay-based aerogels.[44] Pojanavaraphan et al. demonstrated a remarkable improvement in the mechanical properties of casein/clay aerogels through cross-linking of the polymer and formation of a 3-D network structure.[45] Similar approach was used in the present study to cross-link the PVA chains as well as the CNF and GONS nanoentities. Figure 4 shows the specific compressive strength

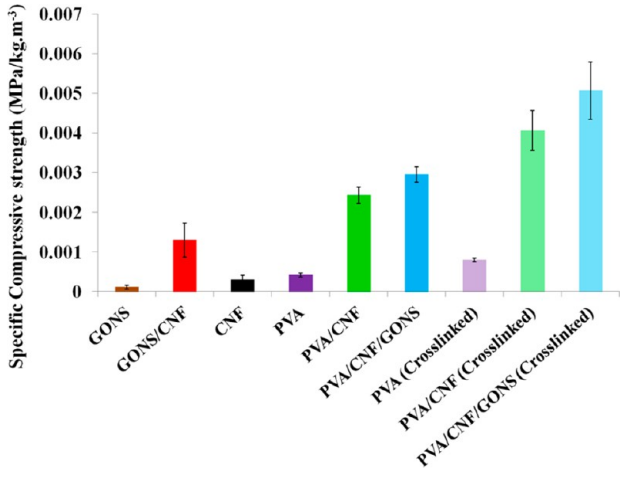

Figure 4. Specific compressive strengths of the aerogels made of various formulations consisting of CNFs, GONSs, and PVA that were either cross-linked or non-cross-linked.

of the aerogels made of various formulations consisting of CNFs, GONSs, and PVA that were either cross-linked or non-cross-linked. The specific compressive strength of the PVA/CNF/GONS aerogel was considerably higher than that of the neat CNF aerogel (more than 9 fold) and GONS aerogel (more than 29 fold). It was also significantly higher than aerogels made of GONS/CNF (more than 4 fold) or PVA (more than 6 fold).

Microstructures of the PVA/CNF/GONS Aerogels. Figure 5a−c show the SEM images of the CNF, PVA, and PVA/CNF/GONS aerogels prepared by the freeze-drying

dx.doi.org/10.1021/am400171y | ACS Appl. Mater. Interfaces 2013, 5, 5969−5975

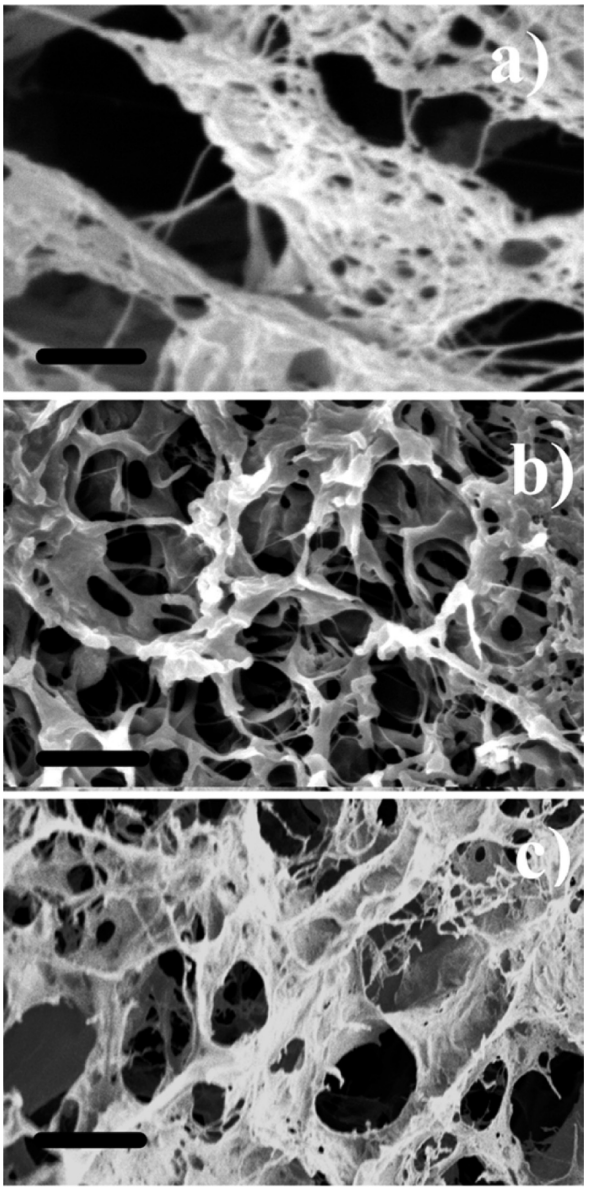

Figure 5. SEM images of (a) CNF, (b) cross-linked PVA, and (c) cross-linked PVA/CNF/GONS aerogels prepared via the freeze-drying method (scale bar: 2 μm).

method, respectively. All three types of aerogels exhibited an interconnected spongelike porous structure with pore sizes ranging from several hundreds of nanometers to a few micrometers. The microstructure of the CNF aerogel exhibited a hierarchical structure; i.e., there are scattered regions with lower aerogel densities which form open micrometer-sized channels. During the freeze-drying process, nucleation and growth of large ice crystals can occur within the network that pushed out the CNF from its original location. Subsequent sublimation of these large crystals led to the formation of micrometer-sized pores in the aerogels. The sublimation of these large ice crystals also resulted in the collapse of the CNF 3D network structure and the formation of scattered interconnected 2D sheetlike networks. The formation of such hierarchical structures in CNF aerogels has been previously reported by several groups.[31,21]

For the PVA aerogels (Figure 5b), the pores were qualitatively more uniform and had smaller diameters compared to those of CNF aerogel (Figure 5a). This might be attributed to the covalent bonding between the PVA chains and the formation of a 3D network structure which does not collapse upon sublimation. For the PVA/CNF/GONS aerogels, as shown in Figure 5c, their porous structures were more uniform and their average pore sizes were smaller than those of the CNF aerogels.

Surface Wettability and Swelling Properties of the PVA/CNF/GONS Aerogels. Pristine PVA/CNF/GONS aerogels are superhydrophilic and they tend to absorb moisture and swell in water because of the high density of the hydroxyl groups present at the surfaces of the PVA, CNFs, and GONSs.[16] To obtain hydrophobic surfaces, we functionalized the hydroxyl groups on the surface of the PVA/CNF/GONS aerogel structures with silane compounds in the gaseous phase through a simple chemical vapor deposition method. Two silane compounds (silane 1, tridecafluoro-1,2,2-tetrahydrooctyl-trichlorosilane; and silane 2, 4-trifluoromethyl-tetrafluoro-phenyl triethoxysilane) were studied as the coating material and the resulting wetting and swelling properties were evaluated (cf. Figures 6 and 7).

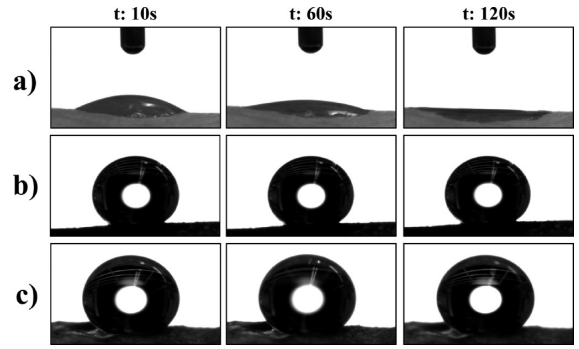

Figure 6. Contact angle measurements of (a) pristine PVA/CNF/GONS aerogels, (b) PVA/CNF/GONS aerogels treated with silane 1, and (c) PVA/CNF/GONS aerogels treated with silane 2 using water droplets.

As shown in Figure 6a, for the pristine PVA/CNF/GONS aerogel (i.e., before silane treatment), the water droplets showed a very small contact angle ($\theta \approx 28.3°$ at $t = 10$ s) and were readily absorbed within the aerogel structure in less than 100 s. In contrast, surface treatment by both silane 1 and silane 2 drastically increased the contact angles of the water droplets on the surface of PVA/CNF/GONS aerogels ($\theta \approx 139.2°$ and $\theta \approx 143.6°$ for silane 1 and silane 2, respectively, at $t = 10$ s). As can be seen in Figures 6b, c, the water droplets maintained their initial contact angles as well as their round shapes on the silane-treated aerogel surfaces, and were not absorbed by the aerogel structures after 120 s. These observations clearly indicate that highly hydrophobic surfaces were formed after silane treatment.[46−51]

Figure 7 demonstrates the water swelling behavior of the cross-linked and non-cross-linked PVA/CNF/GONS aerogels before and after silane treatment. Before silane treatment, the non-cross-linked PVA/CNF/GONS aerogels were not stable in water and fell apart shortly after submersion in water. However, cross-linked PVA/CNF/GONS aerogels were stable in water and their 3D structures did not disintegrate after submersion in water due to the formation of a highly cross-linked PVA network. As can be seen in Figure 7a, prior to silane treatment, cross-linked PVA/CNF/GONS aerogels absorbed water to

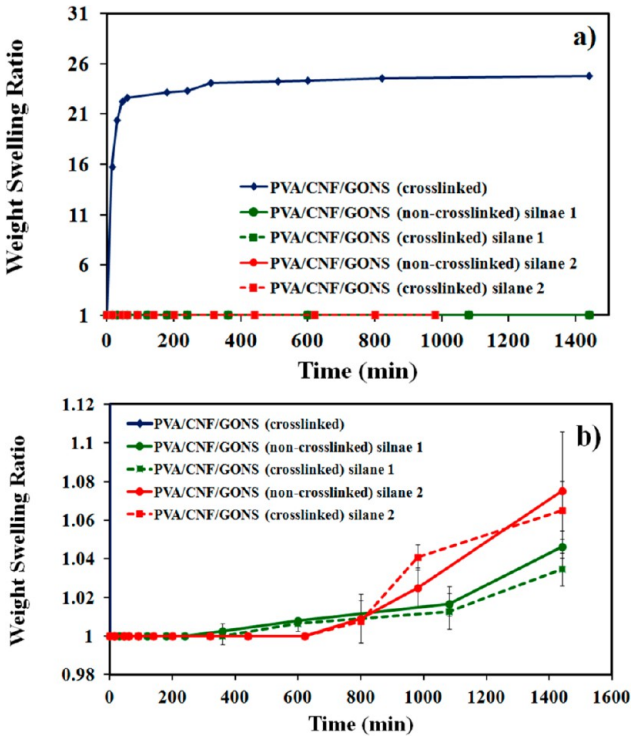

Figure 7. (a) Swelling characteristics of the PVA/CNF/GONS aerogels before and after silane treatment. (b) Magnified version of a.

more than 2300% of its initial weight after being submersed in water for 5 h. This can be attributed to the presence of hydroxyl groups on the surface of the aerogel and its superhydrophilic nature as previously demonstrated by contact angle measurements.[16]

However, after silane treatment (both silane 1 and silane 2), the non-cross-linked PVA/CNF/GONS aerogels not only were stable in water, but also demonstrated a minimum amount of swelling (4.6% for silane 1 and 7.5% for silane 2) after being submersed in water for 24 h. The improved stability of the non-cross-linked PVA/CNF/GONS aerogel structures can be attributed to the formation of a thin and interpenetrated silane coating network on the surface of the aerogel that is also highly hydrophobic.[52] Moreover, the hydrophobic nature of the fluoro groups on the surface of the silane coatings renders the silane-treated PVA/CNF/GONS aerogels highly hydrophobic as previously shown by contact angle measurements.[46−51] In addition, as shown in Figure 7b, after silane treatment, the cross-linked PVA/CNF/GONS aerogels demonstrated slightly less water swelling (3.4% for silane 1 and 6.5% for silane 2) as compared to their non-cross-linked counterparts.

Finally, it may be worth pointing out that the compressive strengths of the PVA/CNF/GONS aerogels before and after silane treatment were also compared and it was found that statistically, silanization did not cause any significant difference in mechanical properties.

Thermal Conductivity and Thermal Stability of the PVA/CNF/GONS Aerogels. For certain applications, particularly for thermal insulation applications, ultralow thermal conductivities and high thermal stabilities are desirable. The thermal conductivity of the PVA/CNF/GONS aerogels was 4.53×10^{-2} ($\pm$ 0.01×10^{-2}) W m^{-1} K^{-1} at ambient conditions. The high porosity (>90%) and small-sized pores possessed by the aerogels resulted in a drastically lower thermal conductivity in comparison with their solid counterparts. This is due to the fact that thermal transportation in aerogels is mainly governed by the gaseous phase (air), whose thermal transportation rate is significantly lower than that of the solid phase and/or radiation.[30,53,54]

Thermal transport in aerogel occurs via gaseous conduction, solid conduction, and infrared radiative transfer. Solid conduction increases with increasing density whereas gaseous conduction and infrared radiative transfer decreases with increasing density. Simulations as well as experiments have shown that the thermal conductivity of aerogels decreases at ultralow densities with increasing density until it reaches a minimum at densities ranging from 75 to 125 kg/m^3 (depending on the aerogel material) and then increases with increasing density.[55]

The thermal stability of the cross-linked and non-cross-linked PVA/CNF/GONS aerogels were examined before and after silane treatment using thermogravimetric analysis. As shown in Figure 8, one significant weight loss step was observed for all the samples. However, for nonsilane-treated aerogels, cross-linked PVA/CNF/GONS aerogels demonstrated considerable improvement in thermal stability over their non-cross-linked

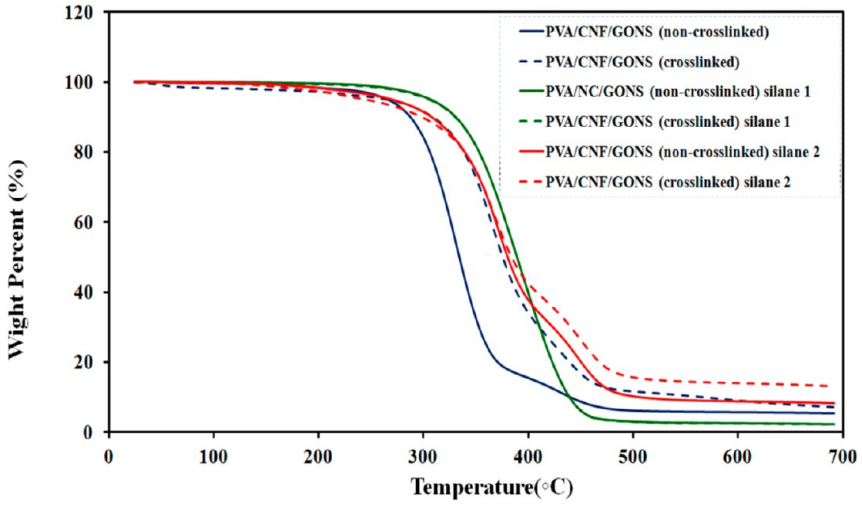

Figure 8. PVA/CNF/GONS aerogels' weight loss as a function of temperature.

counterparts. For example, the temperatures corresponding to 20% weight loss for the cross-linked and non-cross-linked PVA/CNF/GONS aerogels were 337 and 305 °C, respectively. The better thermal stability exhibited by the cross-linked samples may be attributed to the formation of extra carbon−carbon bonds as the result of aerogel network cross-linking.[56] In addition, surface treatment with both types of silane improved the thermal stability of both non-cross-linked and cross-linked PVA/CNF/GONS aerogels which can be attributed to the retardation of PVA thermal decomposition by covalent bonds formed between PVA and silica. Upon coating the samples with silane 1, the temperatures corresponding to 20% weight loss for the cross-linked and non-cross-linked PVA/CNF/GONS aerogels shifted to higher temperatures (339 °C for both cross-linked and non-cross-linked). The thermal stability improvement corresponding to a 20% weight loss for cross-linked and non-cross-linked PVA/CNF/GONS aerogels after treatment with silane 2 was 353 and 343 °C, respectively.

BET Surface Area Measurements of the PVA/CNF/GONS Aerogels. The average BET specific surface area of the PVA/CNF/GONS aerogels was 220 ± 44 m^2/g, which was lower than that of the GONS (495 ± 41 (m^2/g)), PVA/GONS (243 ± 57 (m^2/g)), and CNF/GONS (358 ± 30 (m^2/g)) aerogels, but was higher than that of CNF (140 ± 15 (m^2/g)), PVA (80 ± 8 (m^2/g)), and PVA/CNF (190 ± 36(m^2/g)) aerogels (c.f. Figure 9).

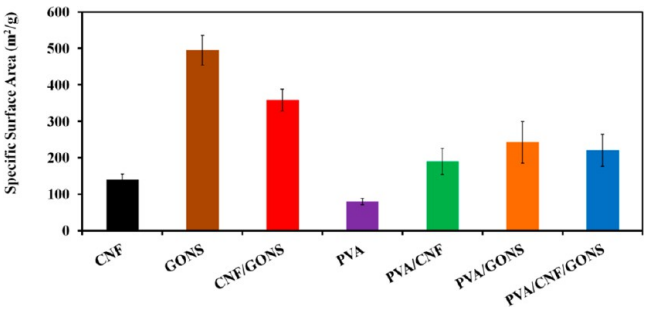

Figure 9. BET specific surface areas of CNF, GONS, PVA aerogels, and their composites.

The incorporation of two different nanofillers (i.e., CNFs and GONSs) with high specific surface areas[16,57] increased the surface area of the PVA/CNF/GONS aerogels significantly in comparison with the PVA aerogels. Both CNFs and GONSs are nanofillers that can yield ultrahigh surface areas depending on the level of exfoliation of the nanofillers and consequently accessible surfaces for gas adsorption.[57,58]

CONCLUSIONS

PVA/CNF/GONS hybrid organic aerogels with ultralow densities (<35 kg/m^3) and excellent material properties were successfully prepared using an environmentally friendly, simple, scalable, and cost-effective method (viz. freeze-drying). Moreover, the surface of the PVA/CNF/GONS aerogel was chemically modified using an easy silane treatment method which produced a hydrophobic surface, thus leading to an extremely low swelling ratio and rate of moisture absorption. These highly porous, lightweight, sustainable aerogels possessed excellent specific compressive strengths and compressive failure strain at very low densities. The thermal conductivity of this aerogel was 0.045 W m^{-1} K^{-1}, which could be further reduced by increasing the density of the aerogel. These hybrid organic aerogels can offer a broad range of properties that make them a cost-effective and environmentally friendly alternative for thermal insulation materials used in housing, clothing, aerospace, and commercial aircraft industry.

ASSOCIATED CONTENT

Supporting Information

A detailed description of the preparation methods for various aerogel formulations and further characterization of CNF and GONS are provided. This material is available free of charge via the Internet at http://pubs.acs.org/.

AUTHOR INFORMATION

Corresponding Author

*E-mail: sgong@engr.wisc.edu.

Notes

The authors declare no competing financial interest.

ACKNOWLEDGMENTS

The authors gratefully acknowledge financial support from the National Science Foundation (CMMI 1032186 and I-Corps) and USDA Forest Products Laboratory (Madison, WI). The authors are also thankful to Professor Eric R. Roden for providing access to the BET surface area analyzer.

REFERENCES

(1) Aaltonen, O.; Jauhiainen, O. *Carbohydr. Polym.* **2009**, *75*, 125−129.
(2) Corma, A. *Chem. Rev.* **1997**, *97*, 2373−2419.
(3) Davis, M. E. *Nature* **2002**, *417*, 813−821.
(4) Dubinin, M. M. *Chem. Rev.* **1960**, *60*, 235−241.
(5) Guo, H.; Nguyen, B. N.; McCorkle, L. S.; Shonkwiler, B.; Meador, M. A. B. *J. Mater. Chem.* **2009**, *19*, 9054−9062.
(6) Nguyen, B. N.; Meador, M. A. B.; Tousley, M. E.; Shonkwiler, B.; McCorkle, L.; Scheiman, D. A.; Palczer, A. *ACS Appl. Mater. Interfaces* **2009**, *1*, 621−630.
(7) Zhang, G. H.; Dass, A.; Rawashdeh, A. M. M.; Thomas, J.; Counsil, J. A.; Sotiriou-Leventis, C.; Fabrizio, E. F.; Ilhan, F.; Vassilaras, P.; Scheiman, D. A.; McCorkle, L.; Palczer, A.; Johnston, J. C.; Meador, M. A. B.; Leventis, N. *J. Non-Cryst. Solids* **2004**, *350*, 152−164.
(8) Capadona, L. A.; Meador, M. A. B.; Alunni, A.; Fabrizio, E. F.; Vassilaras, P.; Leventis, N. *Polymer* **2006**, *47*, 5754−5761.
(9) Meador, M. A. B.; Capadona, L. A.; McCorkle, L.; Papadopoulos, D. S.; Leventis, N. *Chem. Mater.* **2007**, *19*, 2247−2260.
(10) Meador, M. A. B.; Fabrizio, E. F.; Ilhan, F.; Dass, A.; Zhang, G. H.; Vassilaras, P.; Johnston, J. C.; Leventis, N. *Chem. Mater.* **2005**, *17*, 1085−1098.
(11) Meador, M. A. B.; Weber, A. S.; Hindi, A.; Naumenko, M.; McCorkle, L.; Quade, D.; Vivod, S. L.; Gould, G. L.; White, S.; Deshpande, K. *ACS Appl. Mater. Interfaces* **2009**, *1*, 894−906.
(12) Meador, M. A. B.; Malow, E. J.; Silva, R.; Wright, S.; Quade, D.; Vivod, S. L.; Guo, H.; Guo, J.; Cakmak, M. *ACS Appl. Mater. Interfaces* **2012**, *4*, 536−544.
(13) Guo, H.; Meador, M. A. B.; McCorkle, L.; Quade, D. J.; Guo, J.; Hamiltom, B.; Cakmak, M.; Sprpwl, G. *ACS Appl. Mater. Interfaces* **2011**, *3*, 546−552.
(14) Mohite, D. P.; Mahadik-Khanolkar, S.; Luo, H.; Lu, H.; Sotiriou-Leventis, C.; Leventhis, N. *Soft Matter* **2013**, *9*, 1516−1530.
(15) Tan, C.; Fung, B. M.; Newman, J. K.; Vu, C. *Adv. Mater.* **2001**, *13*, 644−646.
(16) Aulin, C.; Netrval, J.; Wagberg, L.; Lindstrom, T. *Soft Matter* **2010**, *6*, 3298−3305.

(17) Chen, W.; Yu, H.; Liu, Q.; Liu, Y.; Li, J. *Soft Matter* **2011**, *7*, 10360−10368.
(18) Zhang, W.; Zhang, Y.; Lu, C.; Deng, Y. *J. Mater. Chem.* **2012**, *22*, 11642−11650.
(19) Carlsson, D. O.; Nystrom, G.; Zhou, Q.; Berglund, L. A.; Nyholm, L.; Stromme, M. *J. Mater. Chem.* **2012**, *22*, 19014−19024.
(20) Sehaqui, H.; Zhou, Q.; Berglund, L. A. *Compos. Sci. Technol.* **2011**, *71*, 1593−1599.
(21) Paakko, M.; Vapaavuori, J.; Silvennoinen, R.; Kosonen, H.; Ankerfors, M.; Lindstrom, T.; Berglund, L. A.; Ikkala, O. *Soft Matter* **2008**, *4*, 2492−2499.
(22) Liu, S.; Yan, Q.; Tao, D.; Yu, T.; Liu, X. *Carbohydr. Polym.* **2012**, *89*, 551−557.
(23) Koukios, E. G.; Valkanas, G. N. *Ind. Eng. Chem. Prod. Res. Dev.* **1982**, *21*, 309−314.
(24) Millett, M. A.; Baker, A. J.; Satter, L. D. *Biotechnol. Bioeng.* **1975**, 193−219.
(25) Turbak, A. F.; Snyder, F. W.; Sandberg, K. R. *J. Appl. Polym. Sci.* **1983**, *37*, 815−827.
(26) Iwamoto, S.; Abe, K.; Yano, H. *Biomacromolecules* **2008**, *9*, 1022−1026.
(27) Paakko, M.; Ankerfors, M.; Kosonen, H.; Nykanen, A.; Ahola, S.; Osterberg, M.; Ruokolainen, J.; Laine, J.; Larsson, P. T.; Ikkala, O.; Lindstrom, T. *Biomacromolecules* **2007**, *8*, 1934−1941.
(28) Henriksson, M.; Henriksson, G.; Berglund, L. A.; Lindstrom, T. *Eur. Polym. J.* **2007**, *43*, 3434−3441.
(29) Saito, T.; Hirota, M.; Tamura, N.; Kimura, S.; Fukuzumi, H.; Heux, L. *Biomacromolecules* **2009**, *10*, 1992−1996.
(30) Husing, N.; Schubert, U. *Angew. Chem., Int. Ed.* **1998**, *37*, 23−45.
(31) Matsumura, S.; Kurita, H.; Shimokobe, H. *Biotechnol. Lett.* **1993**, *15*, 749−754.
(32) Marcano, D. C.; Kosynkin, D. V.; Berlin, J. M.; Sinitskii, A.; Sun, Z. Z.; Slesarev, A.; Alemany, L. B.; Lu, W.; Tour, J. M. *ACS Nano* **2010**, *4*, 4806−4814.
(33) Randall, J. P.; Meador, M. A. B.; Jana, S. C. *ACS Appl. Mater. Interfaces* **2011**, *3*, 613−626.
(34) Gross, J.; Fricke, J. *Nanostruct. Mater.* **1995**, *6*, 905−908.
(35) Alhassan, S. M.; Qutubuddin, S.; Schiraldi, D. A. *Langmuir* **2010**, *26*, 12198−12202.
(36) Finlay, K.; Gawryla, M. D.; Schiraldi, D. A. *Ind. Eng. Chem. Res.* **2008**, *47*, 615−619.
(37) Gui, X. C.; Cao, A. Y.; Wei, J. Q.; Li, H. B.; Jia, Y.; Li, Z.; Fan, L. L.; Wang, K. L.; Zhu, H. W.; Wu, D. H. *ACS Nano* **2010**, *4*, 2320−2326.
(38) Leventis, N. *Acc. Chem. Res.* **2007**, *40*, 874−884.
(39) Parmenter, K. E.; Milstein, F. *J. Non-Cryst. Solids* **1998**, *223*, 179−189.
(40) Boday, D. J.; Stover, R. J.; Muriithi, B.; Keller, M. W.; Wertz, J. T.; DeFriend Obrey, K. A.; Loy, D. A. *ACS Appl. Mater. Interfaces* **2009**, *1*, 1364−1369.
(41) Bandi, S.; Bell, M.; Schiraldi, D. A. *Macromolecules* **2005**, *38*, 9216−9220.
(42) Gawryla, M. D.; Van den Berg, O.; Weder, C.; Schiraldi, D. A. *J. Mater. Chem.* **2009**, *19*, 2118−2124.
(43) Bandi, S.; Schiraldi, D. A. *Macromolecules* **2006**, *39*, 6537−6545.
(44) Hostler, S. R.; Abramson, A. R.; Gawryla, M. D.; Bandi, S. A.; Schiraldi, D. A. *Int. J. Heat Mass Transfer* **2009**, *52*, 665−669.
(45) Pojanavaraphan, T.; Magaraphan, R.; Chiou, B. S.; Schiraldi, D. A. *Biomacromolecules* **2010**, *11*, 2640−2646.
(46) Jin, H.; Kettunen, M.; Laiho, A.; Pynnonen, H.; Paltakari, J.; Marmur, A.; Ikkala, O.; Ras, R. H. A. *Langmuir* **2011**, *27*, 1930−1934.
(47) Pan, Q. M.; Wang, M. *ACS Appl. Mater. Interfaces* **2009**, *1*, 420−423.
(48) Pan, Q. M.; Wang, M.; Chen, W. T. *Chem. Lett.* **2007**, *36*, 1312−1313.
(49) Pan, Q. M.; Wang, M.; Wang, H. B.; Zhao, J. W.; Yin, G. P. *Electrochim. Acta* **2008**, *54*, 197−202.
(50) Jiang, Z. X.; Geng, L.; Huang, Y. D. *Mater. Lett.* **2010**, *64*, 2441−2443.
(51) Jiang, Z. X.; Geng, L.; Huang, Y. D.; Guan, S. A.; Dong, W.; Ma, Z. Y. *J. Colloid Interface Sci.* **2011**, *354*, 866−872.
(52) Plueddemann, E. P. *Prog. Org. Coat.* **1983**, *11*, 297−308.
(53) Scheuerpflug, P.; Caps, R.; Buttner, D.; Fricke, J. *Int. J. Heat Mass Transfer* **1985**, *28*, 2299−2306.
(54) Fricke, J. *J. Non-Cryst. Solids* **1990**, *121*, 188−192.
(55) Fricke, J. T. T. *Thin Solid Films* **1997**, *297*, 212−223.
(56) Zhang, X. Q.; Takegoshi, K.; Hikichi, K. *Polymer* **1992**, *33*, 718−724.
(57) Dreyer, D. R.; Park, S.; Bielawski, C. W.; Ruoff, R. S. *Chem. Soc. Rev.* **2010**, *39*, 228−240.
(58) Heath, L.; Thielemans, W. *Green. Chem.* **2010**, *12*, 1448−1453.